

Insights into the Biochemical and Geochemical Interplay in CO₂/H₂ Underground Bio-methanation

Lin Wu^{1,2*}, Zhengmeng Hou¹, Tao Zhu³

1 Institute of Subsurface Energy Systems, Clausthal University of Technology, Clausthal-Zellerfeld 38678, Germany; 2 National Key Laboratory of Oil and Gas Reservoir Geology and Exploitation, Southwest Petroleum University, Chengdu 610500, China; 3 School of Chemical & Environmental Engineering, China University of Mining & Technology (Beijing), Beijing 100083, China.

(*Corresponding Author: lin.wu@tu-clausthal.de)

ABSTRACT

CO₂/H₂ underground bio-methanation (UBM) technology offers considerable promise because of its versatile functions. However, alongside biocatalysts methanogens, sulfate-reducing bacteria (SRB) and acetogens also utilize CO₂/H₂ as substrates, initiating a range of complex geochemical reactions that may impact both the efficiency and safety of the process. To elucidate the complex biochemical and geochemical interplay in UBM, this study utilized an innovative microbial kinetic model that incorporates environmental factors and subsurface space limitations, implemented within the geochemical simulation platform PHREEQC. This framework facilitated the analysis of scenarios where methanogens, acetogens, and SRB exist individually within different mineral systems, enhancing understanding of each microbe's influence. Building on this, the study further examined complex interactions when all three microbes are present together, as well as the effects of reservoir temperature and gas pressure. The results indicate that both methanogen and SRB metabolism tend to raise the pH of formation water, while acetogen metabolism has the opposite effect. When all three microbes are present, the buffering effect of carbonate minerals enhances methanogen activity, causing a rise in pH during CO₂/H₂ conversion, which leads to the re-dissolution of hydrogen sulfide gas produced by SRB into the formation water, thereby reducing safety risks. Ultimately, CH₄ makes up as much as 96% of the gas phase. Additionally, when the temperature is near the optimal growth range for methanogens, the conversion rate is rapid; however, the competitive consumption of CO₂ and H₂ by acetogens also intensifies. Moreover, an increase in the total pressure of CO₂ and H₂ results in a lower pH in the formation water. This shift suppresses methanogen

function, lowering the conversion efficiency and causing a greater proportion of CO₂ and H₂ to be transformed into acetate. The findings of this study contribute to understanding the complex biochemical and geochemical interplay in UBM and provide guidance for selecting sites and optimizing design in UBM projects.

Keywords: Biogeochemical interaction; Carbon circular utilization; Large-scale energy storage; Renewable natural gas; Underground bio-methanation

1. INTRODUCTION

Global climate change is becoming increasingly severe, making the control of greenhouse gas emissions a focal point for countries worldwide [1]. While renewable energy and energy efficiency are crucial for emission reduction, numerous studies indicate that these methods alone are inadequate to achieve the Paris Agreement's goal [2, 3]. In this context, artificial negative-carbon technologies have emerged as essential supplements for achieving carbon neutrality [4, 5]. Among these, Carbon Capture, Utilization, and Storage (CCUS) is considered one of the most promising strategies [6]. This technology not only facilitates geological carbon sequestration but also improves the recovery and efficiency of underground resources and energy, such as oil and gas, effectively reducing the cost of carbon sequestration [7-9].

In recent years, CCUS technology has evolved toward multi-pathway synergy, integrating with H₂, biological, and geothermal technologies to create innovative negative-carbon utilization models [10-12]. These developments provide crucial support for building a clean, low-carbon, safe, and efficient future energy system. Among these innovative technologies, CO₂/H₂

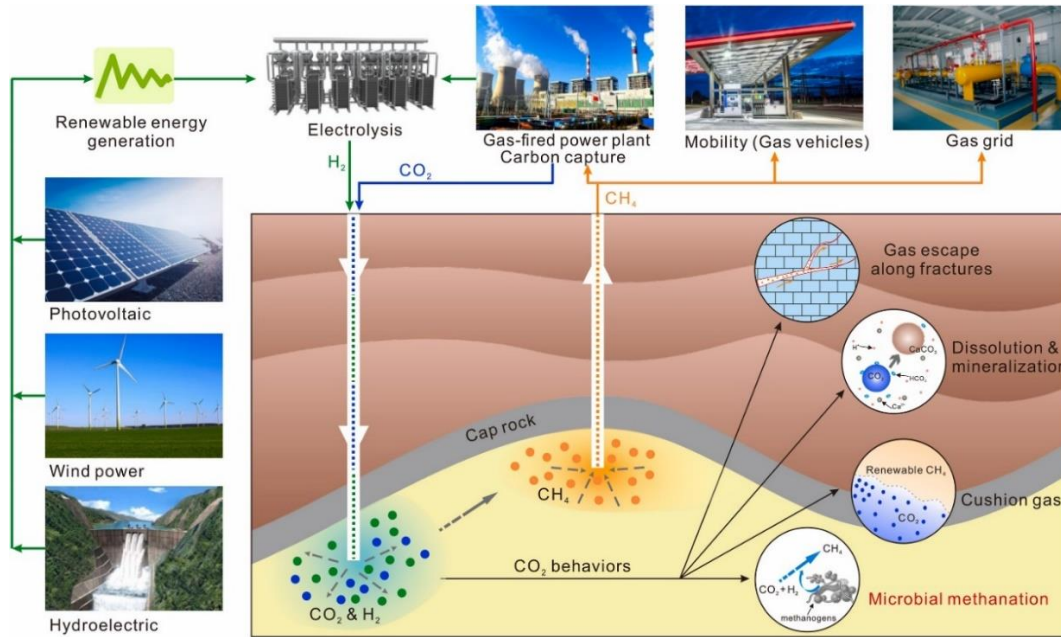


Fig. 1. Schematic diagram of CO₂/H₂ underground bio-methanation [15].

underground bio-methanation stands out for its multifunctionality (Fig. 1) [13, 14]. This technology involves injecting CO₂ and H₂ into depleted oil and gas reservoirs, where methanogens convert the gases into CH₄, which is stored in situ to meet energy peak-shaving needs [15, 16]. Additionally, part of the CO₂ can be geologically sequestered through dissolution, mineralization, and other methods [17]. Thus, the technology enables carbon circular utilization and sequestration, large-scale underground energy storage, and the synthesis of renewable natural gas, offering significant potential for sustainable development and the circular carbon economy [18, 19].

Currently, several studies have explored this technology. For example, Hellerschmied et al. [20] confirmed its viability and long-term stability through 16 conversion experiments. Khajooie et al. [21] conducted batch experiments to explore how rock pore characteristics, like specific surface area and porosity, affect conversion efficiency. Additionally, some research delves into bio-hydrodynamic behaviors. Eddaoui et al. [22], for instance, developed a bio-hydrodynamic model that includes microbial adsorption and desorption to evaluate bio-clogging caused by methanogenesis. Hogeweg et al. [23] looked into the potential of using a multicomponent multiphase coupling model to enhance methanogenesis by injecting freshwater into high-salinity reservoirs. Nikolaev et al. [24] examined the influence of reservoir and operational parameters on UBM. Wu et al. [25] studied the intricate biogeochemical

interactions when only methanogens are present in UBM.

It is important to note that, in addition to methanogens, other microorganisms can also utilize injected CO₂ or H₂ as substrates [26, 27]. However, the metabolic dynamics of these microbes and their complex biogeochemical interactions within the UBM context have not been thoroughly studied, and their potential impacts on the efficiency and safety of UBM technology remain unclear. Therefore, this paper employs a novel microbial kinetic model integrated into the geochemical software PHREEQC to explore these complex biogeochemical interactions.

2. METHODOLOGY

Firstly, the Dual-Monod model, which simultaneously considers electron donor and acceptor limitations, is applied to characterize the specific growth rate of microbes [28]:

$$\mu_{gr} = \mu_{max} \frac{C_A}{C_A + K_A} \frac{C_D}{C_D + K_D} \quad (1)$$

where μ_{gr} represents the specific growth rate, and while μ_{max} its maximum value without substrate limitation. C_A and C_D refer to the electron acceptor and donor concentrations, respectively, while K_A and K_D are the related half-saturation constants. The impact of the reservoir environment is calculated using the following expression [29].

$$\mu_{max} = \mu_{opt} \psi_T \psi_{pH} \psi_s \quad (2)$$

where μ_{opt} represents the optimal specific growth rate; ψ_T , ψ_{pH} , and ψ_s are dimensionless impact coefficients

that correspond to the temperature, pH, and salinity, respectively [30].

The rate of substrate consumption is determined by the specific growth rate of the microbe (μ_{gr}), the yield coefficient (Y), and the biomass (N):

$$r_s = -\frac{\mu_{gr}}{Y} N \quad (3)$$

Additionally, microbes in the subsurface are constrained by pore space, preventing unlimited growth [31]. Therefore, the model also introduces a capacity factor (F_x):

$$F_x = 1 - \frac{N}{N_{max}} \quad (4)$$

where N_{max} is the maximum biomass concentration the environment can support. Consequently, the rate of biomass change (r_{bio}) can ultimately be expressed as:

$$r_{bio} = -r_s F_x Y - dN \quad (5)$$

The aforementioned model has been integrated into the geochemical simulation software PHREEQC V 3.0, and its feasibility and reliability have been verified [30]. Leveraging PHREEQC's robust geochemical simulation capabilities, all relevant models utilize its built-in features, contingent on the selected database [32]. The following simulations primarily use the *phreeqc.dat*. Additionally, mineral precipitation and dissolution are treated as equilibrium reactions [28, 33].

3. SIMULATION SETUP

This study leverages the A1 depleted carbonate gas reservoir in China's Sichuan Basin as a case study. The simulation treats the gas-water-rock system as zero-dimensional [28], meaning gas injection, production, and spatial distribution are not considered; it simulates the shut-in phase following gas injection. In the base scenario, primary minerals are simplified to dolomite and calcite, two fast-reacting minerals, comprising 55 wt% and 45 wt%, respectively. Secondary minerals primarily include brucite. Additionally, a non-carbonate scenario (a pure quartz system) serves as a comparison. For gas composition, the system is considered to contain CO₂, H₂, and CH₄ at respective partial pressures of 30, 120, and 130 atm. The research primarily investigates three microbial groups: methanogenic archaea, acetogenic bacteria, and sulfate-reducing bacteria (SRB). Key kinetic and equilibrium reactions are detailed in Table 1, while the environmental requirements for these microbes are outlined in Table 2. The simulation duration is 720 days.

4. RESULTS AND DISCUSSION

To deepen the understanding of complex biogeochemical interactions, the section first examines the individual metabolism of methanogens, acetogens, and SRB, followed by their interactions when all three microbial groups coexist. Moreover, the effects of

Table 1. Key kinetic and equilibrium reactions in the simulation process [32-34].

Microbial metabolism / Equilibrium phase	Reaction equations	Equilibrium constant (25 °C, 1bar)
Kinetic reactions		
Methanogenesis	$\text{HCO}_3^- + 4\text{H}_{2(\text{aq})} + \text{H}^+ \rightarrow \text{CH}_{4(\text{aq})} + 3\text{H}_2\text{O}$	Not applicable
Acetogenesis	$2\text{HCO}_3^- + 4\text{H}_{2(\text{aq})} + \text{H}^+ \rightarrow \text{C}_2\text{H}_3\text{O}_2^- + 4\text{H}_2\text{O}$	Not applicable
Sulfate reduction	$\text{SO}_4^{2-} + 4\text{H}_{2(\text{aq})} + \text{H}^+ \rightarrow \text{HS}^- + 4\text{H}_2\text{O}$	Not applicable
Equilibrium reactions		
H ₂	$\text{H}_{2(\text{g})} \leftrightarrow \text{H}_{2(\text{aq})}$	-3.1050
CO ₂	$\text{CO}_{2(\text{g})} \leftrightarrow \text{CO}_{2(\text{aq})}$	-1.468
CH ₄	$\text{CH}_{4(\text{g})} \leftrightarrow \text{CH}_{4(\text{aq})}$	-2.8502
H ₂ S	$\text{H}_{2\text{S}(\text{g})} \leftrightarrow \text{H}^+ + \text{HS}^-$	-7.9759
Acetate	$\text{C}_2\text{H}_3\text{OOH} \leftrightarrow \text{C}_2\text{H}_3\text{O}_2^- + \text{H}^+$	-4.7572
Calcite	$\text{CaCO}_3(\text{s}) \leftrightarrow \text{CO}_3^{2-} + \text{Ca}^{2+}$	8.48
Dolomite	$\text{CaMg}(\text{CO}_3)_2(\text{s}) \leftrightarrow \text{Ca}^{2+} + \text{Mg}^{2+} + 2\text{CO}_3^{2-}$	-17.09
Brucite	$\text{Mg}(\text{OH})_2(\text{s}) + 2\text{H}^+ \leftrightarrow \text{Mg}^{2+} + 2\text{H}_2\text{O}$	16.2980

Table 2 Environmental requirements for microbial growth [33, 35, 36].

Microbes	pH			Temperature (°C)			Salinity (g/L)	
	Min	Opt	Max	Min	Opt	Max	Opt	Max
Methanogens	4.1	7.7	10.2	10	45	122	<60	200
Acetogens	3.6	7.04	9.5	25	38	72	<40	300
SRB	1	7.01	11.5	10	48	113	<100	240

reservoir temperature and CO₂/H₂ total pressure are discussed.

4.1 Analysis of microbial metabolism

4.1.1 Methanogenesis

In the carbonate environment, the injection and dissolution of acidic gases lowered the pH of the formation water from an initial 6.2 to 5.0 (Fig. 2). Although this pH level is below the optimal range for methanogen reproduction, the salinity remains within an acceptable range, and the impact of temperature is minimal. Consequently, methanogens maintain a comparatively high reproduction rate, with a significant increase in biomass observed after 20 days, reaching approximately 0.04 g/L by around 60 days. In this investigation, the upper biomass limit for methanogens in the subsurface environment was defined as 0.05 g/L. As this concentration is approached, spatial constraints increasingly inhibit microbial proliferation, leading to a pronounced decline in their growth rate and signaling the onset of a quasi-stationary phase. During substrate consumption, a gradual reduction in gas pressure is observed, accompanied by an increase in water mass. Around day 430, when the available dissolved inorganic carbon (DIC) is fully depleted, methanogen activity shifts predominantly into a decay phase.

Additionally, prior to the full depletion of DIC, the steady increase in pH enhances the dissociation of H₂CO₃, creating conditions favorable for the precipitation of carbonate minerals. Consequently, the rate of calcite dissolution diminishes over time, initially driven by the system's tendency to reach equilibrium, while dolomite precipitation progressively intensifies. When DIC is depleted, a sharp rise in pH triggers the precipitation of brucite, which reduces the Mg²⁺ concentration in the formation water. Consequently, dolomite transitions from precipitation to extensive dissolution, partially replenishing the Ca²⁺ in the formation water. Furthermore, the significant increase in pH leads to continued calcite precipitation throughout the process.

In the non-carbonate scenario, the system lacks the capacity to neutralize acidity, leading to an initial decline in pH to approximately 4.4, which is close to the minimum threshold for methanogen survival, significantly inhibiting their growth. As a result, even after 200 days, the biomass of methanogens only increases modestly, reaching just 0.023 g/L by 720 days. This limited growth means that the typically observed changes associated with methanogen activity, such as gas pressure drop, DIC consumption, and increased water content, are less pronounced compared to the calcite-dolomite system. Moreover, as the water content increases, there is a slight rise in the amount of dissolved

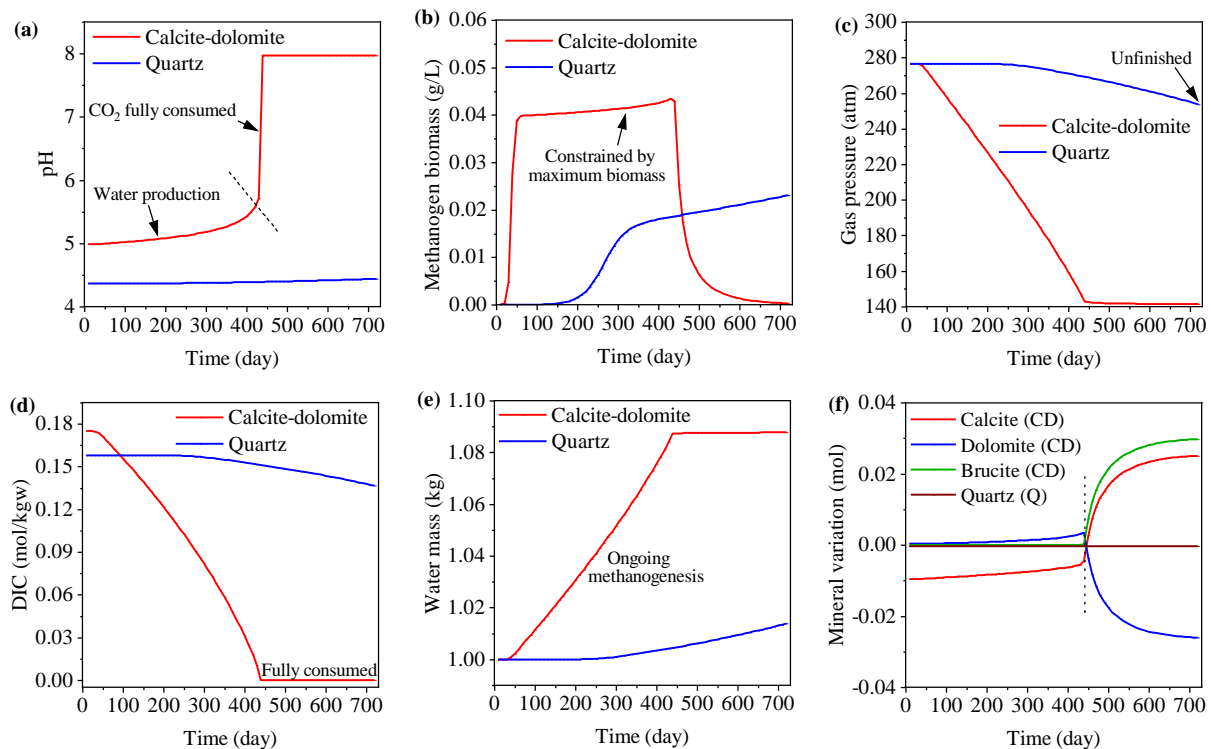


Fig. 2. Evolution of key parameters over time with only methanogens present. "CD" denotes the calcite–dolomite system, while "Q" refers to the pure quartz system. The same notation applies in subsequent figures.

quartz, from 3.52×10^{-4} mol to a final 3.56×10^{-4} mol, although this change is not significant.

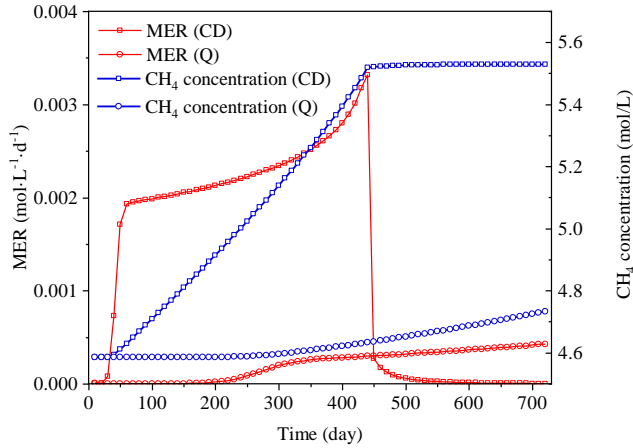


Fig. 3. Dynamic changes in MER and CH₄ concentration with only methanogens present.

Regarding CH₄ production in the calcite-dolomite system, the trend of methane evolution rate (MER) aligns with the growth pattern of methanogen biomass (Fig. 3). Although biomass growth slows after 60 days, MER continues to increase at a relatively rapid pace. This is primarily due to the shift in pH from acidic to neutral and slightly alkaline levels, caused by methanogenic

metabolism, creating a more favorable environment for methanogen reproduction. As a result, the dynamic MER reaches a peak of 3.32×10^{-3} mol·L⁻¹·d⁻¹. When CO₂ in the gas phase is consumed, the MER drops sharply but does not fall directly to zero. This is because, although the biomass is in a decay stage, it has not been completely depleted. Additionally, the carbon provided by the dissolution of dolomite can still be converted directly into CH₄. Consequently, the final CH₄ content reaches 5.53 mol/L. In the pure quartz system, MER only shows a significant increase after 200 days and remains at a low level, reaching a maximum of 0.43×10^{-3} mol·L⁻¹·d⁻¹. This results in a relatively small increase in CH₄ content.

4.1.2 Acetogenesis

In the carbonate environment, the biomass of acetogens begins to increase significantly around 100 days (Fig. 4), reaching a peak of 0.035 g/L by approximately 300 days, after which it remains largely unchanged. The maximum biomass of acetogens is smaller than that of methanogens, primarily because acetogens have a lower specific growth rate compared to methanogens. This difference also accounts for the significantly slower increase in acetogen biomass. Additionally, acetogen metabolism consumes CO₂ and H₂

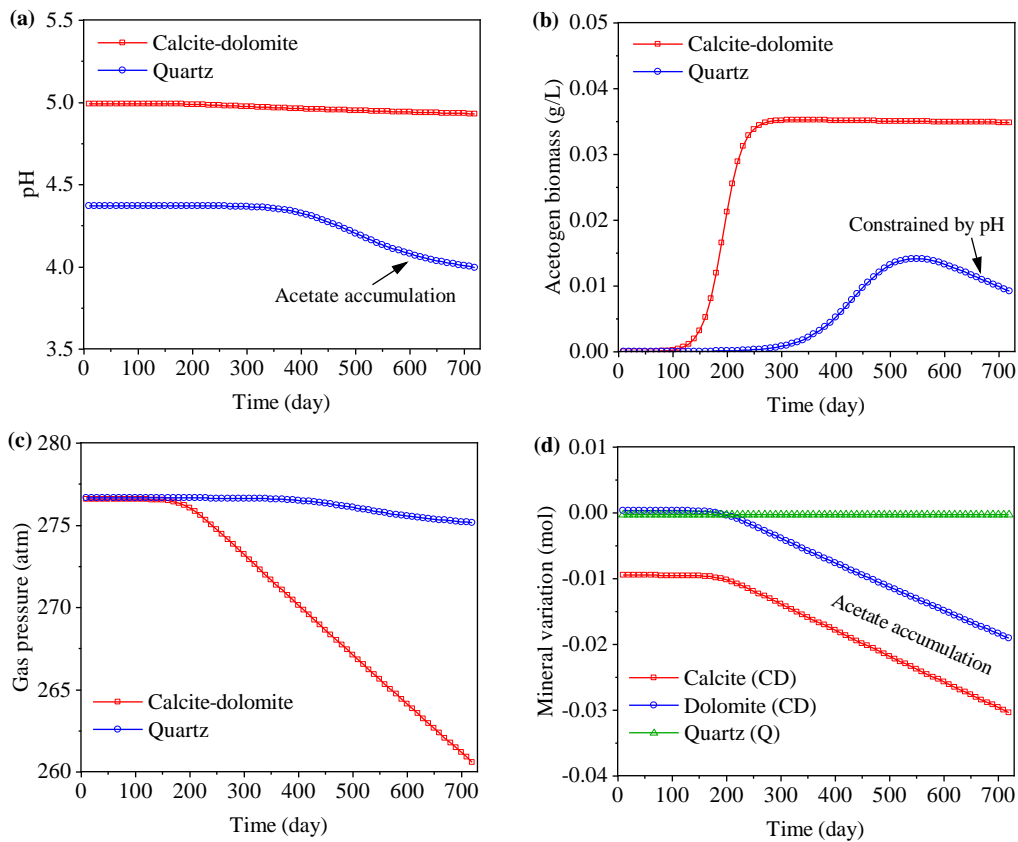


Fig. 4. Evolution of key parameters over time with only acetogens present.

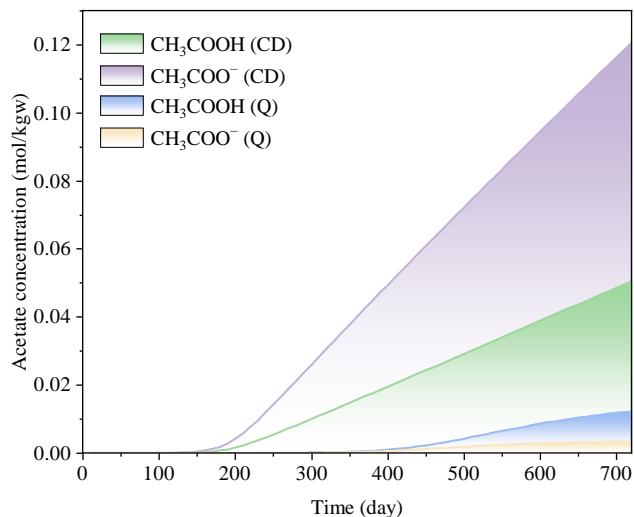


Fig. 5. Evolution of acetate concentration over time with only acetogens present.

in the gas phase. This process results in a pressure drop to a final level of 260.6 atm. Given that the temperature is close to the upper limit for acetogen reproduction at 72 °C, which is not conducive to their optimal reproduction, the overall metabolic rate is relatively slow. Moreover, the dissolution of calcite and dolomite imparts a strong buffering effect to the formation water, resulting in minimal changes in pH, yet their dissolution

continues to increase. Since the system remains in acidic conditions, no brucite formation occurs.

Finally, the total acetate concentrations reach 0.17 mol/kgw and 0.016 mol/kgw, respectively (Fig. 5). It is important to note that in the calcite-dolomite system, acetate predominantly exists as CH_3COO^- due to the relatively stable pH that favors ionization. In contrast, in the non-carbonate environment, the excessive buildup of H^+ suppresses the ionization of CH_3COOH . As a result, a greater proportion of acetate exists as CH_3COOH molecules rather than as ions in this system.

4.1.3 Sulfate reduction

Since SRB are highly acid-resistant, with the ability to thrive at pH levels as low as 1, the initial pH differences between the calcite-dolomite system and the pure quartz system do not significantly affect their growth rates in the early stages (Fig. 6). However, after about 50 days, as biomass begins to increase significantly, the growth rate of SRB in the calcite-dolomite system becomes slightly faster, reaching a maximum after approximately 130 days. It's important to note that SRB use SO_4^{2-} as an electron acceptor. Given the initial concentration of S(6) is 1.47×10^{-3} mol/kgw and compounds such as MgSO_4 and CaSO_4 form, the

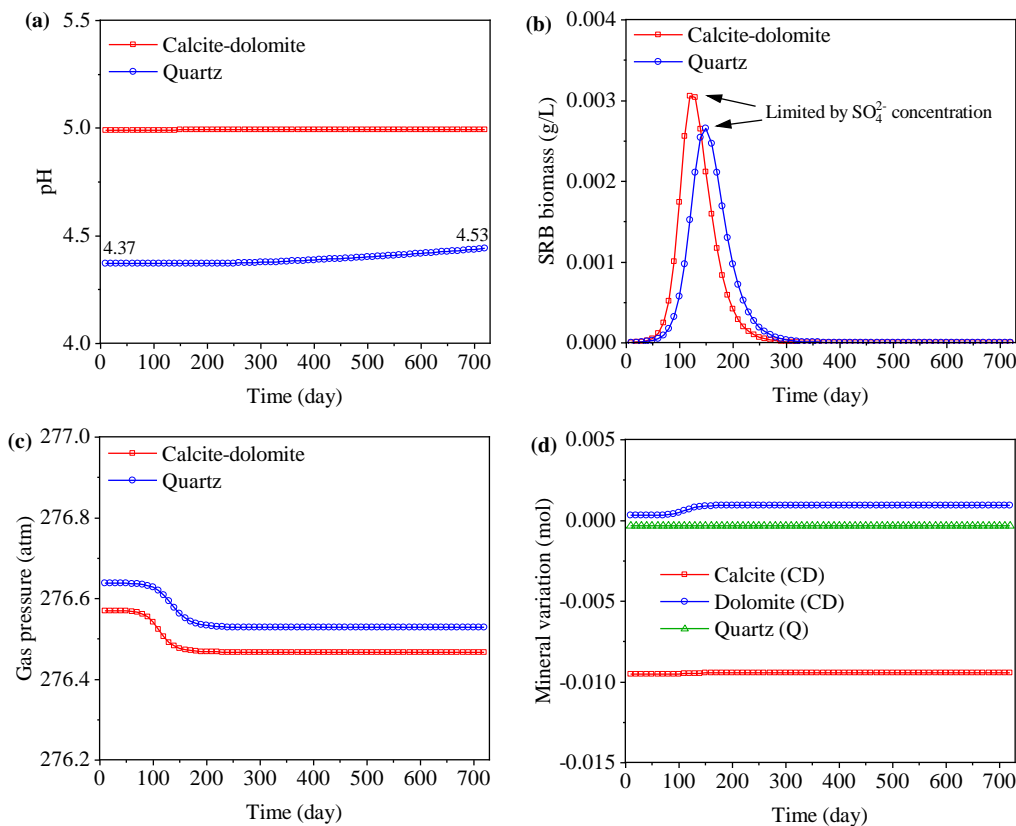


Fig. 6. Evolution of key parameters over time with only SRB present.

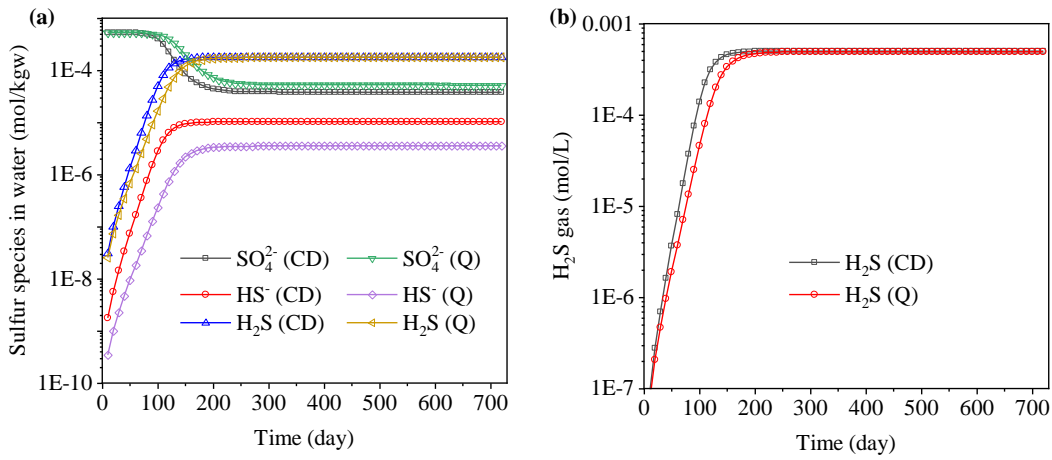


Fig. 7. Evolution of sulfur species over time in (a) water and (b) gas.

concentration of SO₄²⁻ is lowered to only 5.4 × 10⁻⁴ mol/kgw. Consequently, the maximum biomass of SRB is limited to about 3 × 10⁻³ g/L. Moreover, the gas pressure drop resulting from SRB metabolism is minimal, amounting to only 0.103 atm. Although a small amount of water production causes a slight increase in the concentration of OH⁻, the presence of calcite and dolomite maintains the system's alkalinity, keeping the pH essentially constant. In the pure quartz system, the growth rate of SRB is slightly reduced, making the impact of decay on biomass more pronounced. Consequently, the maximum biomass is also lower. Without the buffering effect of minerals like calcite and dolomite, the pH experiences a slight increase from 4.37 to 4.53.

Due to slightly enhanced SRB activity in the carbonate environment, the remaining concentration of SO₄²⁻ in the aqueous phase is marginally lower than that observed in the non-carbonate system (Fig. 7). Additionally, H₂S production in both the liquid and gas phases occurs more rapidly in the calcite-dolomite system. Interestingly, despite these differences in activity, the final H₂S concentrations in both systems are nearly identical, reaching 1.8 × 10⁻⁴ mol/kgw in the liquid

phase and 5 × 10⁻⁴ mol/L in the gas phase. However, because the pH is higher and the H⁺ concentration is lower in the calcite-dolomite system, H₂S more readily dissociates into HS⁻ and H⁺. Consequently, the HS⁻ concentration in the calcite-dolomite system is significantly higher than in the pure quartz system, with final values of 1.03 × 10⁻⁵ mol/kgw and 3.53 × 10⁻⁶ mol/kgw, respectively. Regarding S²⁻, since its concentration is less than 1 × 10⁻¹¹ mol/kgw in both systems, it is omitted from the figure.

4.1.4 Three microbial metabolisms

Within the carbonate environment, abundant methanogens convert most of the injected CO₂ into CH₄, achieving a final utilization ratio of about 84% (Fig. 8). Acetogens, which are comparatively less active, convert about 8% of CO₂ into acetate. Altogether, 12% of CO₂ is used by all three microbial types for biomass creation. Moreover, nearly 42% of introduced H₂ is converted into CH₄, below the Sabatier reaction's theoretical 50%, primarily because of uptake by acetogens and SRB. Around 3% of H₂ supports microbial cell growth, while

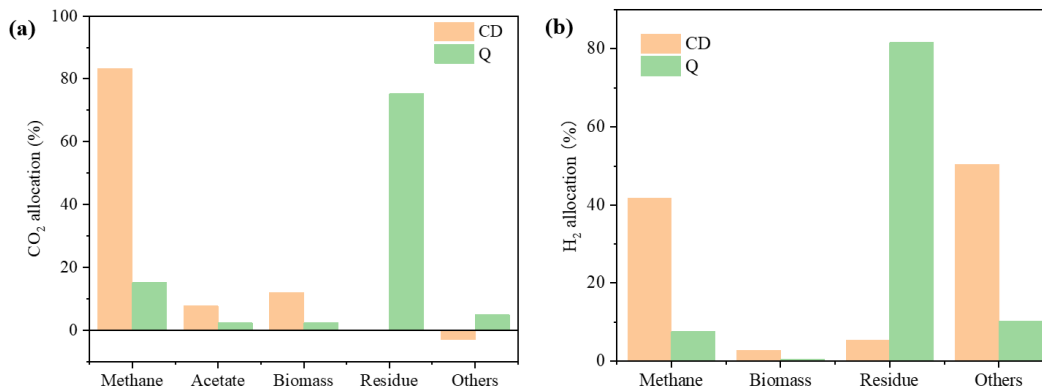


Fig. 8. CO₂ and H₂ allocation at 720 days with three types of microbes present.

roughly half is used to form H₂O, H₂S, acetate, and other compounds. In the pure quartz system, all three microbial activities are reduced, resulting in 75% of CO₂ and 82% of H₂ remaining unutilized.

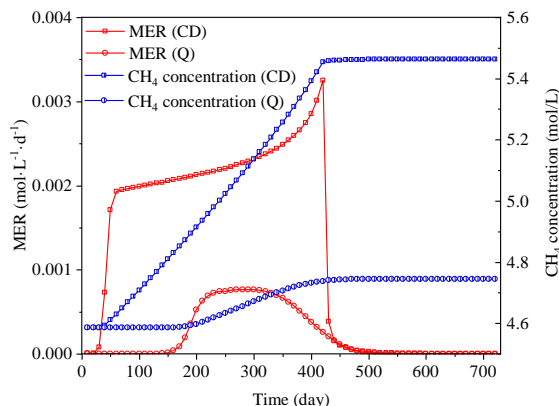


Fig. 9. Dynamic changes in MER and CH₄ concentration over time with three types of microbes present.

Additionally, in the calcite-dolomite system, since methanogens still dominate, the change trend of MER is no different from that when methanogens exist alone (Fig. 9). However, due to the competitive consumption of CO₂ by acetogens, the final CH₄ concentration slightly decreases from 5.53 mol/L to 5.46 mol/L. In the pure quartz system, MER first increases slightly, reaches 7.65×10^{-4} mol·L⁻¹·d⁻¹ after 290 days, and then begins to decrease, falling to 0 at around 500 days, because the biomass of methanogens also tends to 0 at this time, and the final CH₄ content can only reach 4.74 mol/L.

Moreover, within the carbonate environment, CH₄ ultimately constitutes 96% of the gaseous mixture (Fig. 10). This is because the study simplifies the reservoir into a batch system, also considering the initial CH₄ as cushion gas. If the spatial distribution and flow of the gas are factored in, this value would likely decrease, necessitating further study. The rapid increase in the proportion of H₂S in the gas phase between 50 and 150

days is mainly due to SRB metabolism. From 150 to 410 days, while SRB metabolism essentially completes, the proportion of H₂S continues to rise due to the consumption of large amounts of CO₂ and H₂, peaking at 79.2 ppm at 410 days. Thereafter, as the pH of the formation water rises rapidly, it promotes the ionization of H₂S, leading to its redissolution in the formation water and a subsequent reduction to 9.9 ppm in the gas phase. In the pure quartz system, because CO₂ and H₂ are not fully converted, the final proportion of CH₄ reaches only 52.6%. Additionally, since the pH remains at a low level, the S(-2) species in the water phase predominantly exists as H₂S, leading to a final H₂S concentration in the gas phase of 54.1 ppm. Therefore, even if the initial SO₂-4 concentration in the formation water is relatively low, an acidic environment in the formation water can still present significant safety risks due to SRB metabolism. This potential hazard must be regarded with serious concern.

4.2 Effect of reservoir temperature

Fig. 11 illustrates the results at various reservoir temperatures. Although the initial pH is highest at 30°C, methanogen activity is slightly stronger at 50°C, as 50°C is closest to their optimal propagation temperature of 45°C. The gas pressure drops fastest, and dolomite dissolves significantly due to the large amount of DIC consumed in the metabolic process and the precipitation of brucite caused by the increase in pH. SRB is also more active at 50°C, with S(-2) levels initially rising slowly, then increasing sharply in the water due to the pH increase and the redissolution of H₂S in the gas phase. In contrast, acetogens are more active at 30°C, producing more acetate through metabolism, reaching a maximum value of 0.59 mol/kgw at 280 days. However, they struggle to reproduce at 70°C and die off directly at 90°C.

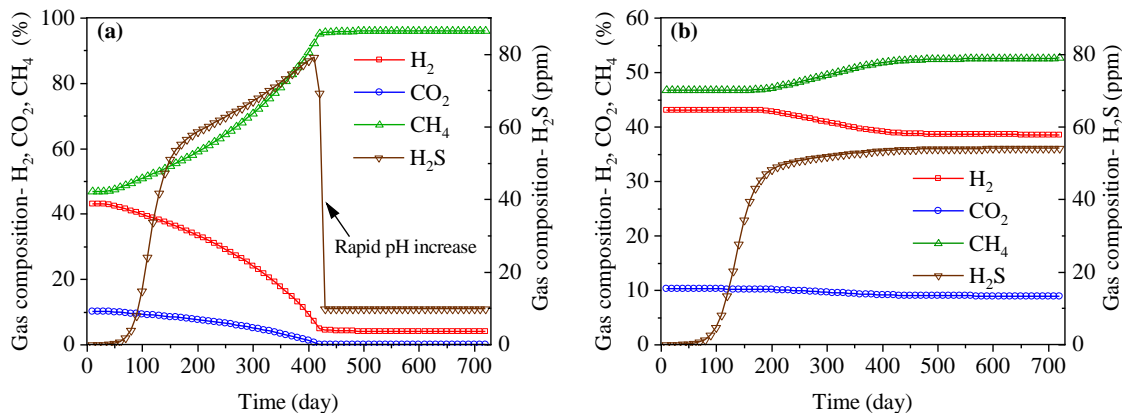


Fig. 10. Evolution of gas composition over time with three types of microbes present in (a) carbonate and (b) non-carbonate environment.

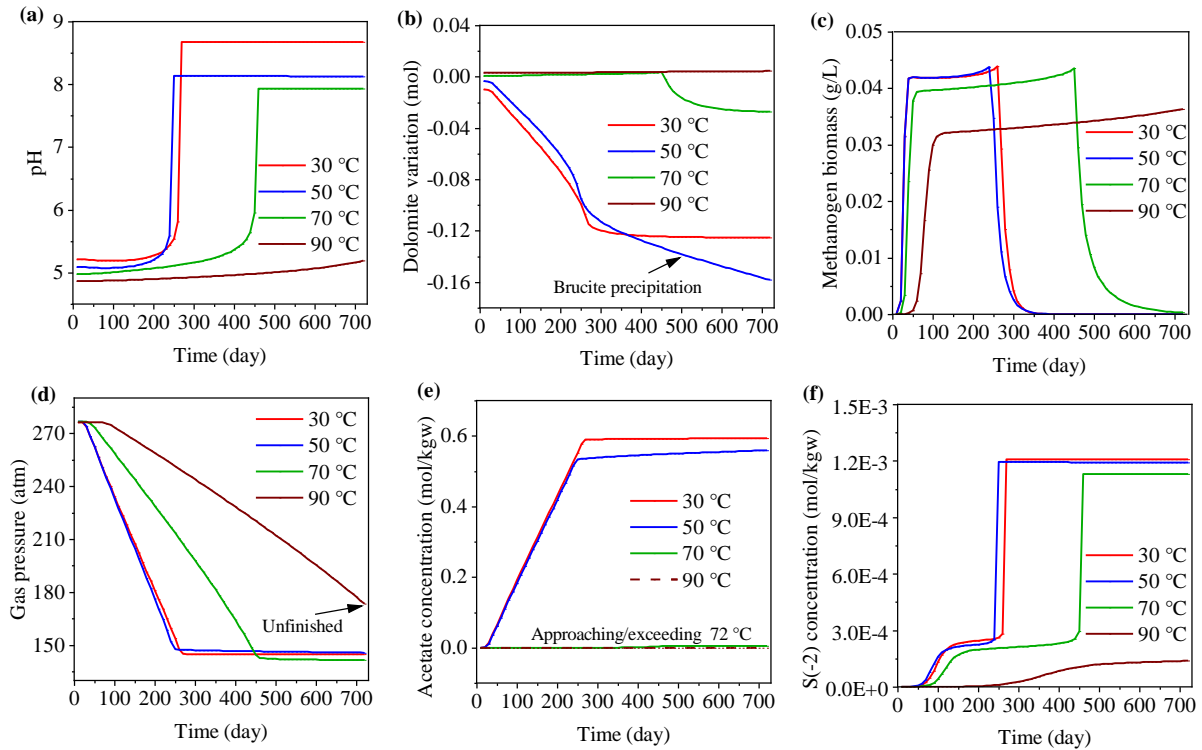


Fig. 11. Evolution of key parameters over time under different reservoir temperatures.

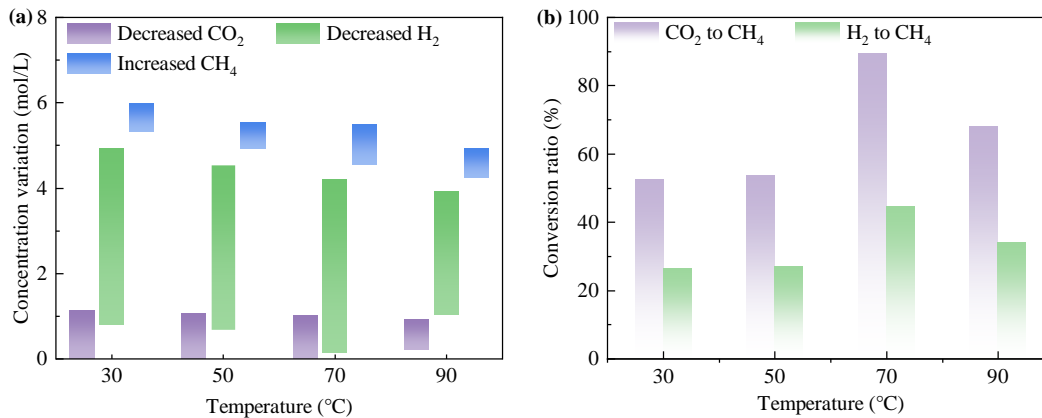


Fig. 12. Impact of reservoir temperature on CO₂/H₂ bio-methanation.

When the partial pressure of the gas remains constant, the gas state equation indicates that the higher the temperature, the smaller the amount of the corresponding gas will be. For example, with temperature rising from 30 °C to 90 °C, the initial concentration of CO₂ decreases from 1.13 mol/L to 0.93 mol/L (Fig. 12). This effect is even more pronounced for H₂ and CH₄, with their concentrations dropping by nearly 1 mol/L. At 30 °C, only 52.5% of CO₂ is converted to CH₄ because acetogens compete and consume a large amount of CO₂ (44.9%) in this low-temperature range. The H₂ conversion rate is only 26.2%. The C/H consumption does not align with the stoichiometric ratio of the Sabatier reaction, resulting in a residual H₂ concentration of 0.8 mol/L when CO₂ is completely

consumed in the gas phase. This discrepancy also helps explain the low conversion ratio observed at 50 °C. Upon reaching 70 °C, the activity of acetogens is severely restricted, allowing 89.4% of CO₂ and 44.7% of H₂ to be transformed into CH₄. The residual H₂ also decreases significantly, reaching a minimum of 0.13 mol/L. At 90 °C, less CO₂ and H₂ are converted, mainly due to slower metabolism.

4.3 Effect of gas pressure

This section explores how total CO₂/H₂ pressure influences conversion by varying their pressures between 70 and 150 atm, while maintaining a fixed CO₂:H₂ ratio of 1:4. The overall gas pressure is held

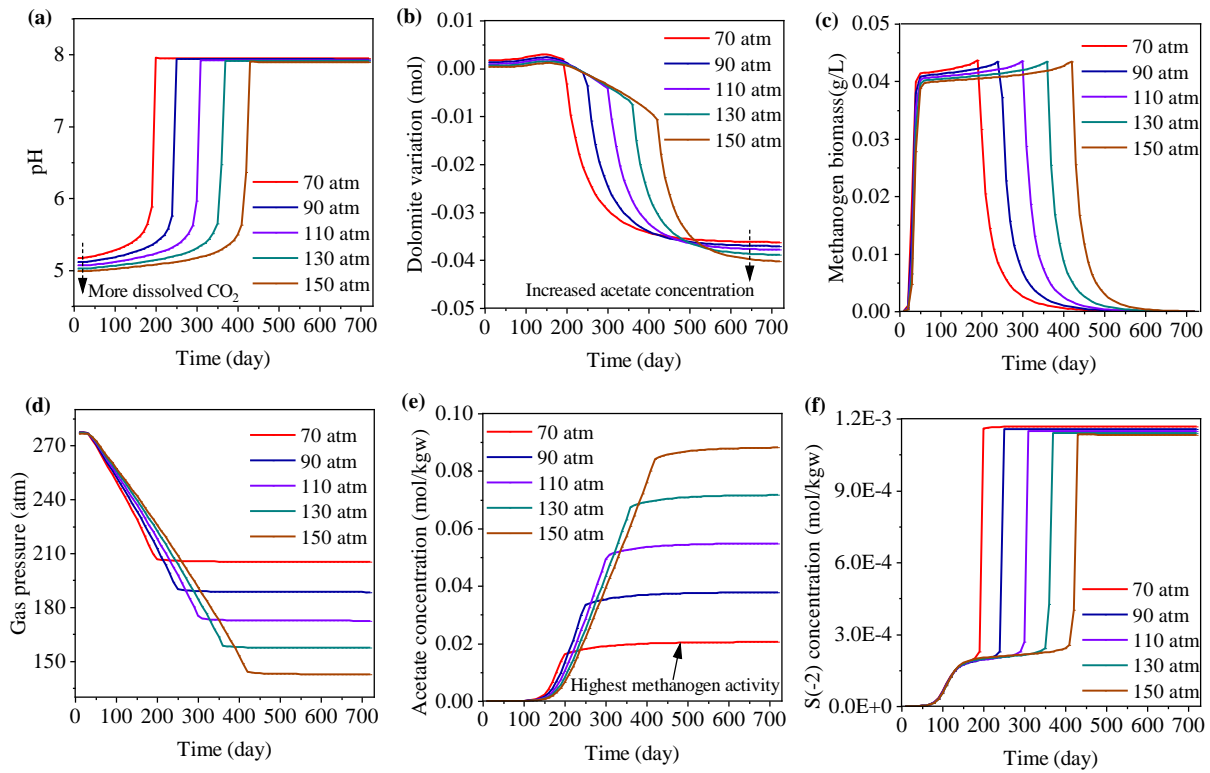


Fig. 13. Evolution of key parameters over time under different total CO₂/H₂ pressures.

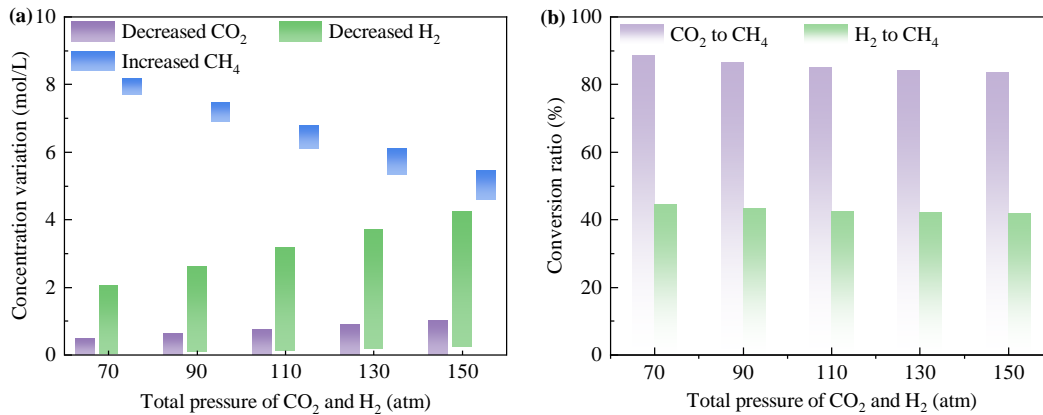


Fig. 14. Impact of gas pressure on CO₂/H₂ bio-methanation.

constant at 280 atm, with CH₄ partial pressure adjusted accordingly. The results are shown in Fig. 13.

As the substrate gas pressure rises from 70 atm to 150 atm, the CO₂ partial pressure also increases, leading to a drop in pH after the system reaches its initial equilibrium, and the amount of dolomite precipitation decreases slightly (Fig. 13). Due to the pH decrease, both methanogen biomass accumulation and gas utilization rates exhibit a noticeable slowdown, extending the time until gas pressure no longer significantly decreases from 200 days to about 420 days. Since the pH stays in an acidic environment for a longer duration, the restriction on methanogen activity is prolonged, promoting the conversion of CO₂ to acetate and increasing the final

accumulated acetate concentration from 0.021 mol/kgw to 0.088 mol/kgw. This also leads to an increase in the amount of dolomite dissolved in the end. Since the gases are injected at a 1:4 ratio, the pH eventually rises to nearly the same level, resulting in the maximum methanogen biomass and the final S(-2) concentration across different total pressures being nearly identical, with no significant differences.

When the pressure is 70 atm, the CO₂ methanation ratio reaches 88.5% after CO₂ is completely consumed (Fig. 14). However, as the pressure increases to 150 atm, the activity of acetogens is relatively enhanced, and only 83.4% CO₂ can be converted into CH₄. Furthermore, since the C/H consumption ratio by acetogens is higher than

the stoichiometric C/H ratio in the Sabatier reaction, the residual gaseous H₂ increases from nearly zero to 0.22 mol/L. This also leads to a decrease in H₂ methanation ratio from 44.4% to 41.7%.

5. CONCLUSIONS

Both methanogen and SRB metabolism tend to raise the pH of formation water, while acetogen metabolism has the opposite effect. When all three microbes are present, the buffering effect of carbonate minerals enhances methanogen activity, causing a rise in pH during CO₂/H₂ conversion, which leads to the re-dissolution of H₂S gas produced by SRB into the formation water, thereby reducing safety risks.

When the temperature is near the optimal growth range for methanogens, such as at 30 or 50 °C, the conversion rate is rapid; however, the competitive consumption of CO₂ and H₂ by acetogens also intensifies. Under high-temperature conditions (90 °C), methanogen activity is significantly inhibited, preventing conversion from being completed even after two years.

With the rise in total pressure of CO₂ and H₂, CO₂ partial pressure increases, resulting in a lower pH in the formation water. This shift suppresses methanogen function, lowering the conversion efficiency and causing a greater proportion of CO₂ and H₂ to be transformed into acetate by acetogens.

ACKNOWLEDGEMENT

This work was funded by the European Union's "Horizon Europe programme" – LOC3G (Grant No. 101129729). The first author gratefully acknowledges financial support from the China Scholarship Council (Grant No. 202208080058).

DECLARATION OF INTEREST STATEMENT

The authors declare that they have no known competing financial interests or personal relationships that could have appeared to influence the work reported in this paper. All authors read and approved the final manuscript.

REFERENCE

[1] IEA. CO₂ emissions in 2023. Paris: International Energy Agency; 2024.

[2] Hou Z, Xiong Y, Luo J, Fang Y, Haris M, Chen Q, et al. International experience of carbon neutrality and prospects of key technologies: Lessons for China. *Petroleum Science*. 2023;20(2):893-909.

[3] Chen L, Msigwa G, Yang M, Osman AI, Fawzy S, Rooney DW, et al. Strategies to achieve a carbon neutral

society: a review. *Environmental Chemistry Letters*. 2022;20(4):2277-310.

[4] Hou MZ, Luo J, Huang L, Beck H-P, Mehmood F, Wang Q, et al. Strategies toward carbon neutrality: comparative analysis of China, USA, and Germany. *Carbon Neutral Systems*. 2025;1(1):3.

[5] Zhang Z, Pan S-Y, Li H, Cai J, Olabi AG, Anthony EJ, et al. Recent advances in carbon dioxide utilization. *Renewable and Sustainable Energy Reviews*. 2020;125:109799.

[6] Zhang X, Yang X, Lu X, Chen J. China carbon dioxide capture, utilization, and storage (CCUS) annual report (2023). China Agenda 21 Management Center, Global Carbon Capture and Storage Institute, Tsinghua University; 2023.

[7] Hou Z, Luo J, Xie Y, Wu L, Huang L, Xiong Y. Carbon circular utilization and partially geological sequestration: Potentialities, challenges, and trends. *Energies*. 2022;16(1):324.

[8] Wu L, Hou Z, Luo Z, Xiong Y, Zhang N, Luo J, et al. Numerical simulations of supercritical carbon dioxide fracturing: A review. *Journal of Rock Mechanics and Geotechnical Engineering*. 2023;15(7):1895-910.

[9] Jia Z, Cao R, Pu B, Cheng L, Li P, Awotunde AA, et al. Effects of non-equilibrium phase behavior in nanopores on multi-component transport during CO₂ injection into shale oil reservoir. *Energy*. 2024;307:132614.

[10] Fleming MR, Adams BM, Ogland-Hand JD, Bielicki JM, Kuehn TH, Saar MO. Flexible CO₂-plume geothermal (CPG-F): Using geologically stored CO₂ to provide dispatchable power and energy storage. *Energy Conversion and Management*. 2022;253:115082.

[11] Hou Z, Wu L, Zhang L, Fang Y, Huang L, Cao C, et al. CO₂-based underground biochemical synthesis of natural gas coupled with geothermal energy production: Technology system, challenges, and prospects. *Natural Gas Industry*. 2023;43(11):181-90.

[12] Huang L, Liu Q, Stefeel C, Liu Y, Hu M, Liu S, et al. Generating H₂ during the CO₂ sequestration in basalt formations. *Geomechanics and Geophysics for Geo-Energy and Geo-Resources*. 2025;11(1):4.

[13] Strobel G, Hagemann B, Huppertz TM, Ganzer L. Underground bio-methanation: Concept and potential. *Renewable and Sustainable Energy Reviews*. 2020;123:109747.

[14] Xiong Y, Hou Z, Xie H, Zhao J, Tan X, Luo J. Microbial-mediated CO₂ methanation and renewable natural gas storage in depleted petroleum reservoirs: A review of biogeochemical mechanism and perspective. *Gondwana Research*. 2023;122:184-98.

- [15] Wu L, Hou Z, Luo Z, Fang Y, Mao J, Qin N, et al. Site selection for underground bio-methanation of hydrogen and carbon dioxide using an integrated multi-criteria decision-making (MCDM) approach. *Energy*. 2024;306:132437.
- [16] Xie Y, Wu X, Hou Z, Li Z, Luo J, Lüddeke CT, et al. Gleaning insights from German energy transition and large-scale underground energy storage for China's carbon neutrality. *International Journal of Mining Science and Technology*. 2023;33(5):529-53.
- [17] Wu L, Hou Z, Xie Y, Luo Z, Huang L, Wu X, et al. Carbon capture, circular utilization, and sequestration (CCUS): A multifunctional technology coupling underground biomethanation with geothermal energy production. *Journal of Cleaner Production*. 2023;426:139225.
- [18] Hou Z, Huang L, Xie Y, Wu L, Fang Y, Wang Q, et al. Economic analysis of methanating CO₂ and hydrogen-rich industrial waste gas in depleted natural gas reservoirs. *Energies*. 2023;16(9):3633.
- [19] Wu L, Hou Z, Li Y, Wang W, Cheng L, Lin J, et al. Carbon circular utilization and sequestration in depleted hydrocarbon reservoirs: Towards a carbon-neutral China. *Energy Geoscience*. 2024;6(1):100343.
- [20] Hellerschmied C, Schritter J, Waldmann N, Zaduryan AB, Rachbauer L, Scherr KE, et al. Hydrogen storage and geo-methanation in a depleted underground hydrocarbon reservoir. *Nature Energy*. 2024:1-12.
- [21] Khajooie S, Gaus G, Dohrmann AB, Krüger M, Littke R. Methanogenic conversion of hydrogen to methane in reservoir rocks: An experimental study of microbial activity in water-filled pore space. *International Journal of Hydrogen Energy*. 2024;50:272-90.
- [22] Eddaoui N, Panfilov M, Ganzer L, Hagemann B. Impact of pore clogging by bacteria on underground hydrogen storage. *Transport in Porous Media*. 2021;139:89-108.
- [23] Hogeweg S, Hagemann B, Ganzer L. Simulation of freshwater injection to enable underground bio-methanation in high-saline gas storage formations. *Conference Simulation of freshwater injection to enable underground bio-methanation in high-saline gas storage formations*, vol. 2022. European Association of Geoscientists & Engineers, p. 1-5.
- [24] Nikolaev DS, Moeninina N, Ott H, Bueltemeier H. Investigation of underground bio-methanation using bio-reactive transport modeling. *SPE Russian Petroleum Technology Conference: SPE*; 2021. p. D021S12R03.
- [25] Wu L, Hou Z, Luo Z, Huang L, Xiong Y, Mehmood F, et al. Efficiency assessment of underground biomethanation with hydrogen and carbon dioxide in depleted gas reservoirs: A biogeochemical simulation. *Energy*. 2023;283:128539.
- [26] Wu L, Hou Z, Luo Z, Fang Y, Huang L, Wu X, et al. Impacts of microbial interactions on underground hydrogen storage in porous media: A comprehensive review of experimental, numerical, and field studies. *Petroleum Science*. 2024;21(6):4067-99.
- [27] Dopffel N, Jansen S, Gerritse J. Microbial side effects of underground hydrogen storage – Knowledge gaps, risks and opportunities for successful implementation. *International Journal of Hydrogen Energy*. 2021;46(12):8594-606.
- [28] Veshareh MJ, Thaysen EM, Nick HM. Feasibility of hydrogen storage in depleted hydrocarbon chalk reservoirs: Assessment of biochemical and chemical effects. *Applied Energy*. 2022;323:119575.
- [29] Peleg M. A new look at models of the combined effect of temperature, pH, water activity, or other factors on microbial growth rate. *Food Engineering Reviews*. 2021;14(1):31-44.
- [30] Wu L, Hou Z, Luo Z. Impacts of microbial competition on underground bio-methanation of hydrogen and carbon dioxide: Insights from biogeochemical simulations. *Renewable Energy*. 2025:123458.
- [31] Jin Q. Building microbial kinetic models for environmental application: A theoretical perspective. *Applied Geochemistry*. 2023;158:105782.
- [32] Parkhurst DL, Appelo C. Description of input and examples for PHREEQC version 3—a computer program for speciation, batch-reaction, one-dimensional transport, and inverse geochemical calculations. *US geological survey techniques and methods* 2013. p. 497.
- [33] Shojaee A, Ghanbari S, Wang G, Mackay E. Interplay between microbial activity and geochemical reactions during underground hydrogen storage in a seawater-rich formation. *International Journal of Hydrogen Energy*. 2023;50:1529-41.
- [34] Hemme C, Van Berk W. Hydrogeochemical modeling to identify potential risks of underground hydrogen storage in depleted gas fields. *Applied Sciences*. 2018;8(11):2282.
- [35] Thaysen EM, McMahon S, Strobel GJ, Butler IB, Ngwenya BT, Heinemann N, et al. Estimating microbial growth and hydrogen consumption in hydrogen storage in porous media. *Renewable and Sustainable Energy Reviews*. 2021;151:111481.
- [36] Heinemann N, Alcalde J, Miocic JM, Hangx SJT, Kallmeyer J, Ostertag-Henning C, et al. Enabling large-scale hydrogen storage in porous media – the scientific challenges. *Energy & Environmental Science*. 2021;14(2):853-64.